ORIGINAL ARTICLE

Mesenchymal Stromal Cell Exosomes Ameliorate Experimental Bronchopulmonary Dysplasia and Restore Lung Function through Macrophage Immunomodulation

Gareth R. Willis[1,2], Angeles Fernandez-Gonzalez[1,2], Jamie Anastas[1,3], Sally H. Vitali[2,4], Xianlan Liu[1], Maria Ericsson[3], April Kwong[1], S. Alex Mitsialis[1,2]*, and Stella Kourembanas[1,2]*

[1]Division of Newborn Medicine, Department of Medicine, and [4]Division of Critical Care Medicine, Department of Anesthesia, Perioperative and Pain Medicine, Boston Children's Hospital, Boston, Massachusetts; and [2]Department of Pediatrics and [3]Department of Cell Biology, Harvard Medical School, Boston, Massachusetts

Abstract

Rationale: Mesenchymal stem/stromal cell (MSC) therapies have shown promise in preclinical models of pathologies relevant to newborn medicine, such as bronchopulmonary dysplasia (BPD). We have reported that the therapeutic capacity of MSCs is comprised in their secretome, and demonstrated that the therapeutic vectors are exosomes produced by MSCs (MSC-exos).

Objectives: To assess efficacy of MSC-exo treatment in a preclinical model of BPD and to investigate mechanisms underlying MSC-exo therapeutic action.

Methods: Exosomes were isolated from media conditioned by human MSC cultures. Newborn mice were exposed to hyperoxia (HYRX; 75% O_2), treated with exosomes on Postnatal Day (PN) 4 and returned to room air on PN7. Treated animals and appropriate controls were harvested on PN7, -14, or -42 for assessment of pulmonary parameters.

Measurements and Main Results: HYRX-exposed mice presented with pronounced alveolar simplification, fibrosis, and pulmonary vascular remodeling, which was effectively ameliorated by MSC-exo treatment. Pulmonary function tests and assessment of pulmonary hypertension showed functional improvements after MSC-exo treatment. Lung mRNA sequencing demonstrated that MSC-exo treatment induced pleiotropic effects on gene expression associated with HYRX-induced inflammation and immune responses. MSC-exos modulate the macrophage phenotype fulcrum, suppressing the proinflammatory "M1" state and augmenting an antiinflammatory "M2-like" state, both *in vitro* and *in vivo*.

Conclusions: MSC-exo treatment blunts HYRX-associated inflammation and alters the hyperoxic lung transcriptome. This results in alleviation of HYRX-induced BPD, improvement of lung function, decrease in fibrosis and pulmonary vascular remodeling, and amelioration of pulmonary hypertension. The MSC-exo mechanism of action is associated with modulation of lung macrophage phenotype.

Keywords: bronchopulmonary dysplasia; exosomes; extracellular vesicles; mesenchymal stem cells; macrophages

(Received in original form May 10, 2017; accepted in final form August 29, 2017)

*Senior authors contributing equally to this article.

Supported in part by National Institutes of Health grants R01 HL085446 and R01 HL055454 (S.K.), Charles H. Hood Foundation Major Grants Initiative to Advance Child Health (S.K.), and a United Therapeutics Corp. Sponsored Research grant (S.K. and S.A.M.); J.A. was supported by T32 HD007466 (S.K.).

Author Contributions: G.R.W. participated in study design and execution, data collection, analysis, and manuscript writing; A.F.-G. participated in study design and execution, data collection, and data analysis; J.A. participated in data analysis; S.H.V., X.L., M.E., and A.K. participated in study execution and technical assistance; S.A.M. and S.K. contributed to study design, supervision of study execution, manuscript writing, data analysis, and final article editing and approval.

Correspondence and requests for reprints should be addressed to Stella Kourembanas, M.D., Division of Newborn Medicine, Boston Children's Hospital, 300 Longwood Avenue, Boston, MA 02115. E-mail: stella.kourembanas@childrens.harvard.edu.

This article has an online supplement, which is accessible from this issue's table of contents at www.atsjournals.org.

Am J Respir Crit Care Med Vol 197, Iss 1, pp 104–116, Jan 1, 2018

Originally Published in Press as DOI: 10.1164/rccm.201705-0925OC on August 30, 2017
Internet address: www.atsjournals.org

At a Glance Commentary

Scientific Knowledge of the Subject: With no effective single therapy to prevent or treat bronchopulmonary dysplasia (BPD), a multifactorial chronic lung disease of preterm infants, the need for new therapies is urgent. Mesenchymal stem/stromal cell (MSC) therapy had shown promise in preclinical models of BPD, and recent studies established that one of the main therapeutic vectors of MSCs is found in their secretome and represented by exosomes (extracellular vesicles). The new promise of an efficacious cell-free treatment for BPD dictates the diligent and timely assessment of MSC-exomes' (MSC-exos) therapeutic capacity.

What This Study Adds to the Field: We are the first to show that a bolus dose of purified MSC-exos significantly improved lung morphology and pulmonary development, decreased lung fibrosis, and ameliorated pulmonary vascular remodeling in a neonatal hyperoxia model of BPD. We extend our observations to show that MSC-exo treatment improved pulmonary function test results and alleviated associated pulmonary hypertension. MSC-exos blunt hyperoxia-induced inflammation, in part, via modulation of lung macrophage phenotype.

Bronchopulmonary dysplasia (BPD) is a chronic lung disease occurring almost exclusively in preterm infants requiring mechanical ventilation and oxygen therapy. It is characterized by restricted lung growth (tissue simplification), subdued alveolar and blood vessel development, and impaired pulmonary function. Several BPD outcomes are associated with long-term pulmonary complications, such as abnormal pulmonary function test results and, in moderate to severe cases, secondary pulmonary hypertension (PH) (1–5). With no effective single therapy for preventing or treating developmental lung injuries, the need for new therapies is urgent. A large number of studies have investigated stem cell–based therapies to ameliorate lung injury associated with preterm birth and administration of different stem/progenitor cell types, such as mesenchymal stem/stromal cells (MSCs) (6, 7), endothelial colony-forming cells (8), and human amnion epithelial cells (9), have shown promise in preclinical models for the prevention and/or treatment of BPD and other major sequelae of prematurity (10, 11).

Despite substantial physiologic improvements in the recipient lung after MSC therapy, several preclinical studies noted the absence of significant engraftment of donor cells in the lung, suggesting that the therapeutic mechanism of action may be paracrine or indirect (12, 13). Indeed, we (6, 14) and others (15, 16) have demonstrated that the cell-free conditioned media (CM) of MSCs afforded superior protection over MSCs themselves in preventing alveolar loss in preclinical BPD models. Subsequently, using a hypoxia-induced PH model, we demonstrated that the therapeutic vector in the MSC secretome comprises the extracellular vesicles (EVs) they release (17, 18), and, in particular, the smaller (<150 nm diameter) subpopulation generated through the endocytic pathway, termed exosomes (19).

More recently, administration of MSC-EVs has also been reported to benefit a number of murine lung disease models (15, 20–23; for reviews *see* References 18, 24) and to even be efficacious in an *ex vivo* human lung model (25). However, wide diversity in EV isolation techniques, coupled with poor characterization, may often obfuscate the therapeutic impact of MSC exosome (MSC-exo) formulations, impairing bioavailability and contaminating preparations with pyrogenic nonexosomal material. We undertake here a more detailed characterization of purified exosomes from MSCs derived from human umbilical cord Wharton's jelly (WJMSCs) and bone marrow MSCs (BMSCs), and investigate their efficacy in an experimental model of BPD.

Methods

Animal Model and Experimental Design

Extended description of our hyperoxia (HYRX)-induced BPD model and analytical methods are described in previous publications (6, 14) and in the online supplement. Animal experiments were approved by the Boston Children's Hospital Animal Care and Use Committee.

Exosome Isolation, Purification, and Characterization

Exosomes (EVs 30–150 nm in diameter, expressing markers CD9, CD63, and flotillin-1, and floating at a density of ~1.18 g/ml) were isolated from cell culture supernatants (CM) after 36-hour incubation in serum-free media. After differential centrifugation to clarify cell debris and related apoptotic detritus, CM were concentrated by filtration and exosomes isolated by flotation on an OptiPrep (iodixanol [IDX]) cushion and further characterized. *See* the online supplement for details.

Statistical Analysis

We used ANOVA followed by Bonferroni's multiple comparison test (GraphPad v 6.0; GraphPad Software Inc.). Pearson correlation coefficients were used to explore the strength of the relationship between immunohistochemistry vascular remodeling parameters and physiological indices of PH. Flow cytometry data analyses used FlowJo software v10.2 (TreeStar). Inflammatory marker mRNA levels were assessed by RT-quantitative PCR (qPCR) and expressed relative to cognate normoxic (NRMX) control group average level; significance was considered at P less than 0.05.

For *in vivo* studies, sample size calculations were based on previous work (14), suggesting that detection of a 15% improvement in lung architecture (assessed by mean linear intercept [MLI]), with greater than 90% power at the 5% α level, required a minimum of five animals per group.

Investigators were blinded to experimental groups for histological analysis and physiological measurements.

Results

Purification, Isolation, and Characterization of Exosomes

Flotation of CM from WJMSCs, BMSCs, or human dermal fibroblasts (HDFs) cultures on an IDX cushion allowed for the extraction of exosomes in fraction 9 of the gradient (Figures 1A and 1B). Compared with fractions 6–10, as assessed by

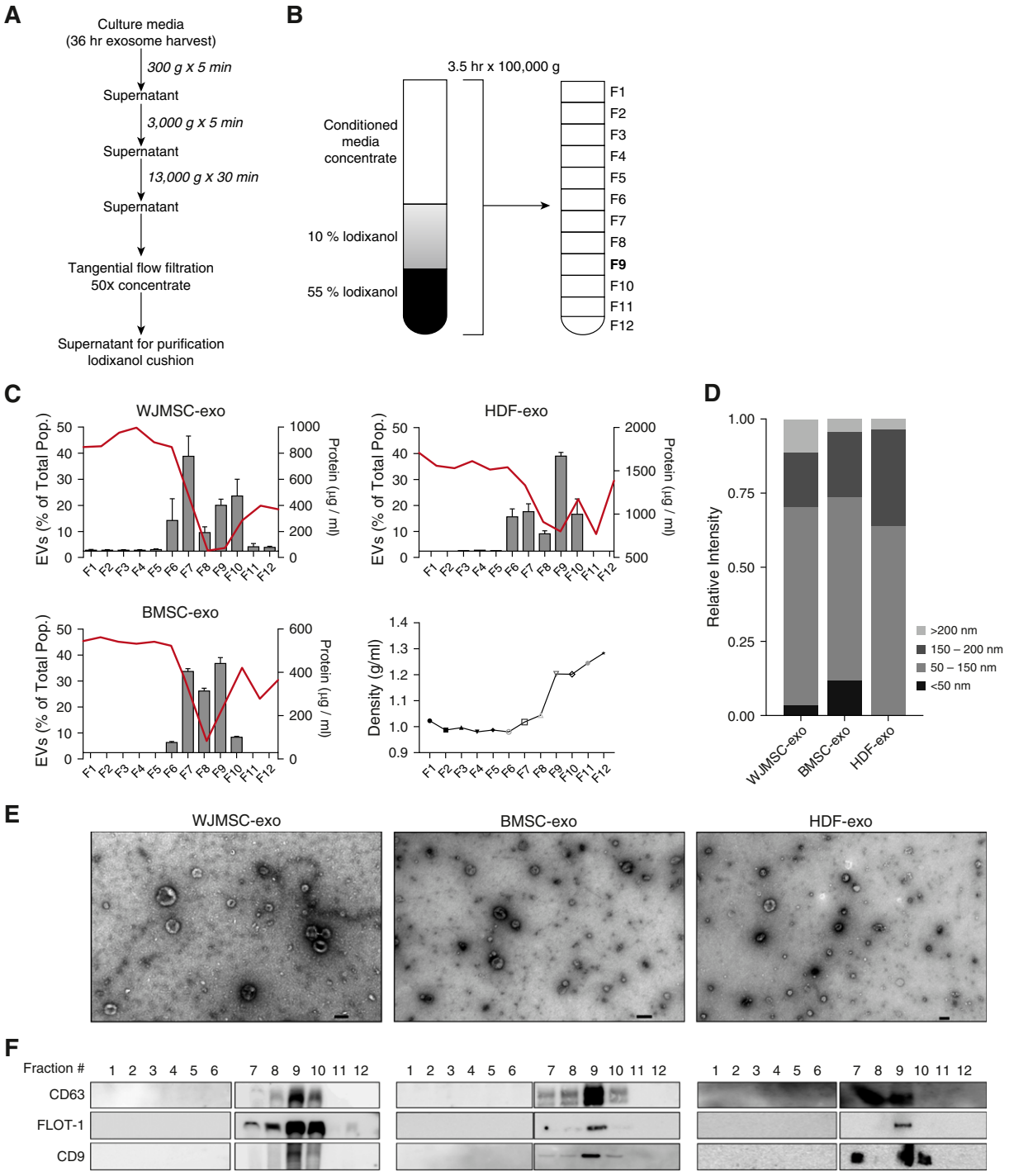

Figure 1. Purification, isolation, and characterization of exosomes. Wharton's jelly mesenchymal stem/stromal cells (WJMSCs), bone marrow MSCs (BMSCs), and human dermal fibroblasts (HDFs) secrete heterogeneous exosome populations. (*A*) To isolate exosomes, conditioned media (CM) were subjected to successive differential centrifugation followed by tangential flow filtration. (*B*) Concentrated (50×) CM was floated on an iodixanol (IDX) cushion gradient to purify and isolate the exosome population (fraction 9, density ~1.18 g/ml). (*C*) Nanoparticle tracking analysis and protein concentration was used to assess exosome concentration and particle:protein ratio in the IDX cushion (12 × 1 ml fractions), respectively. The red line denotes protein concentration, and the bar charts reflect exosome concentration. Fraction density is expressed as grams per milliliter. Each symbol represents a fraction from the Opti-prep cushion gradient. Data are shown as mean ± SEM. (*D*) Representative size distribution of WJMSC exosomes (-exos), BMSC-exos, and HDF-exos isolated from their corresponding fraction 9 gradients. (*E*) Transmission electron microscopy images demonstrating heterogeneous vesicle morphology (high magnification, 30,000×; scale bars = 100 nm). (*F*) The IDX cushion gradient fractions were analyzed by Western blot (fraction 1–6 and 7–12, side by side), using antibodies to proteins representing exosome markers. Equivalent volume of each fraction was loaded per lane. Representative images are shown. As expected for exosome markers, flotillin (FLOT)-1 and tetraspanins (CD63, CD9) were enriched in fraction 9. EVs = extracellular vesicles.

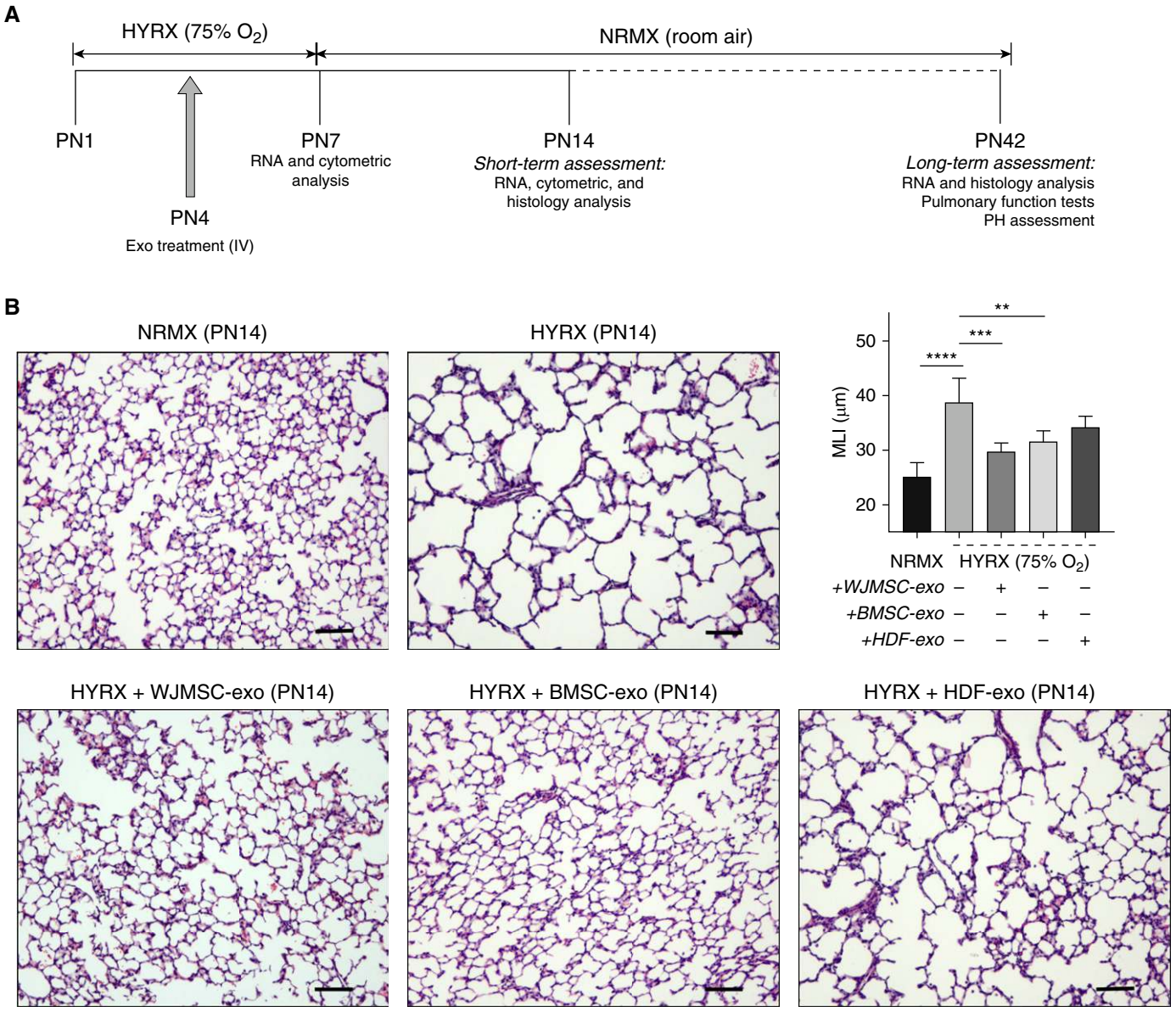

Figure 2. Mesenchymal stem/stromal cell (MSC) exosome (-exo) treatment improves short-term lung architecture outcome. Newborn mice (FVB/NJ strain) were exposed to hyperoxia (HYRX; 75% O_2) for 7 days. HYRX-exposed mice were compared with mice that remained in normoxic (NRMX) conditions (room air). Exosome treatments were delivered intravenously (IV) at Postnatal Day (PN) 4. Short-term outcomes were assessed at PN14 (schematic shown in *A*). Harvested lung sections were stained for hematoxylin and eosin. Images were taken at 100× magnification. HYRX-control and human dermal fibroblast (HDF)-exo–treated mice presented with significant alveolar simplification, characterized by large airspaces and incomplete alveolarization. HYRX-exposed animals that received a bolus dose of either Wharton's jelly MSC (WJMSC)-exos or bone marrow MSC (BMSC)-exos had a markedly improved lung alveolarization when compared with the emphysema-like appearance of the HYRX-control mice. Quantification of mean linear intercept (MLI) represents a surrogate of average air space diameter. Each bar represents an experimental group, indicated on the *x*-axis and by the accompanying (+ or −) symbol. Data represent results from three individual studies. Data are shown as mean ± SEM; $n = 5–15$ per group. $^{**}P < 0.01$, $^{***}P < 0.001$, $^{****}P < 0.0001$. Scale bars = 100 μm. PH = pulmonary hypertension.

transmission electron microscopy (TEM) and nanoparticle tracking analysis (NTA), fraction 9 (at a density of ~1.18 g/ml) boasted a low protein:vesicle ratio, indicating high purity (Figure 1C). TEM and NTA analysis of fraction 9 revealed a heterogeneous exosome population for WJMSC-exo, BMSC-exo, and HDF-exo samples, which occupied a typical diameter of 30–150 nm, had minimal protein aggregate contaminants, and exhibited the distinct biconcave morphological features of exosomes (Figures 1D and 1E). Immunoblots of IDX cushion gradients revealed that fraction 9 for all cell types was positive for CD9, CD63, and flotillin-1 (Figure 1F).

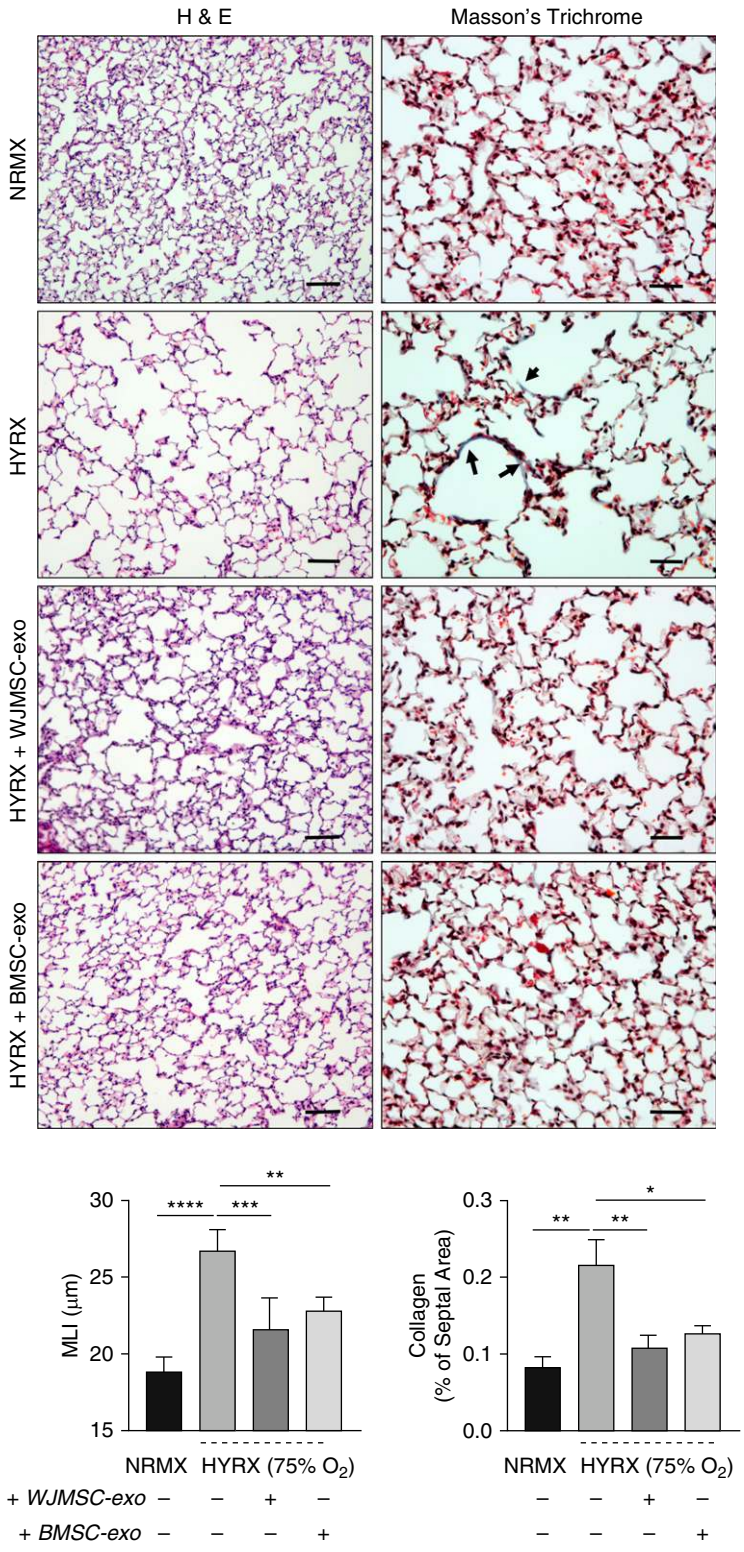

Figure 3. Mesenchymal stem/stromal cell (MSC) exosome (-exo) treatment improves lung architecture and reduces hyperoxia (HYRX)-induced fibrosis. For long-term outcomes, mice were assessed at Postnatal Day 42 (6 wk). Lung sections were stained for hematoxylin and eosin (H&E) and Masson's trichrome to assess the degree of alveolar simplification and fibrosis, respectively. Sections were captured at 100× (H&E) and 200× (Masson's trichrome) magnification using a Nikon Eclipse 80i microscope to illustrate extensive alveolar simplification as well as modest lung fibrosis, denoted

Short-Term Assessment (Postnatal Day 14): A Single Dose of MSC-exos Restores Lung Architecture

Newborn mice were exposed to 75% O_2 (HYRX) from Postnatal Day (PN) 1 to PN7 and returned to room air from PN7 to PN14. Age-matched control litters were housed under standard room air conditions (NRMX). Treatment groups received a single intravenous dose of WJMSC-exos, BMSC-exos, or HDF-exos at PN4 (schematic shown in Figure 2A). At PN14, the HYRX-control group demonstrated a histological pattern reminiscent of human BPD, characterized by severe impairment of alveolar growth, large airspaces, and incomplete alveolar septation (Figure 2B), and this was reflected in elevated MLI values compared with NRMX-control mice (mean ± SEM, 38.7 ± 1 vs. 25.1 ± 1, $P <$ 0.0001, respectively). Animals treated with MSC-exos presented with dramatically improved alveolarization and almost completely restored lung architecture compared with the HYRX-control group. This improvement was observed in treatments with either WJMSC-exos (29.8 ± 1, $P < 0.001$) or BMSC-exos (31.6 ± 2, $P <$ 0.001). HDF-exos served as a biologic and vehicle control, and had no significant protective effect as assessed at PN14 (34.24 ± 2 μm, $P > 0.05$), and were thus not used for experiments assessing long-term effects. No difference was found comparing NRMX-control animals and animals treated with WJMSC-exos under normoxia (*see* Figure E1 in the online supplement; $P > 0.05$).

Long-Term Assessment (PN42): A Single Dose of MSC-exos Improves Pulmonary Development and Ameliorates Septal Fibrosis

To assess long-term endpoints, lung architecture and collagen deposition were measured at PN42 (Figure 3). HYRX-control mice demonstrated persistent destruction of the alveolar architecture, large airspaces, and significant alveolar simplification compared with NRMX-control group (MLI = 26.7 ± 0.7 vs. 18.8 ± 0.5 μm, $P < 0.0001$). Again, animals treated with either WJMSC-exos or BMSC-exos presented a dramatically improved alveolarization and robust restoration of lung architecture when compared with HYRX-control mice (WJMSC-exos, MLI = 21.6 ± 0.9 μm, $P < 0.01$; BMSC-exos, MLI = 22.7 ± 0.4 μm, $P < 0.01$).

Collagen deposition (Masson's trichrome stain) was used to measure the degree of lung fibrosis. Only slight collagen deposition was recorded in all groups in this model of BPD (<1% of total septal area), in comparison to more severe models of BPD where animals were exposed to HYRX for 14 days (14, 18). However, HYRX-control mice had a subtle but significantly higher amount of collagen deposition compared with NRMX-control mice (0.22 ± 0.06 vs. 0.08 ± 0.01 μm, $P < 0.01$, respectively). HYRX-exposed mice treated with either WJMSC-exos or BMSC-exos had significantly decreased collagen deposition (0.1 ± 0.02 and 0.13 ± 0.01 μm, $P < 0.01$, $P < 0.05$, respectively).

MSC-exo Treatment Rescues HYRX-induced Loss of Peripheral Pulmonary Blood Vessels and Peripheral Pulmonary Arterial Remodeling

To explore the potential impact of MSC-exos on HYRX-induced peripheral pulmonary vascular remodeling, lung sections of mice harvested at PN42 were stained with α-smooth muscle actin (Figure 4A). HYRX-exposed animals demonstrated a greater peripheral pulmonary vascular muscularization (36.55 ± 2.7 media thickness index [MTI]) compared with NRMX-control animals (20.23 ± 2.2 MTI; $P < 0.01$). WJMSC-exo and BMSC-exo treatment ameliorated the HYRX-induced vascular muscularization (26.3 ± 1.1 MTI, $P < 0.05$, and 27.22 ± 2.3 MTI, $P < 0.05$, respectively; Figure 4C and Figure E2A).

To determine the effect of HYRX exposure on pulmonary vessel number, we assessed von Willebrand factor staining in lung sections of mice at PN42. Compared with NRMX-control mice, HYRX exposure led to significant loss of small (peripheral) vessels less than 50 μm diameter (4.4 ± 0.3 vs. 2.9 ± 0.2 blood vessels/field, respectively, $P < 0.01$), whereas WJMSC-exo or BMSC-exo treatment restored these vessels (3.9 ± 0.4 and 4.4 ± 0.6 blood vessels/field, $P = 0.06$, and $P < 0.01$, respectively; Figure 4D and Figure E2B). There was no significant difference in number of vessels greater than 150 μm diameter between the groups (data not shown).

MSC-exo Administration Improves HYRX-induced PH

To assess the degree of HYRX-induced PH, right ventricular (RV) systolic pressure (RVSP) measurements, the RV to body weight (BW) ratio (RV:BW) and Fulton's index (RV:left ventricle + septum ratio) were measured. RVSP was found to be modestly elevated in HYRX-control animals (30.8 ± 0.85 vs. 22.38 ± 0.68 mm Hg for NRMX, $P < 0.001$). MSC-exo treatment ameliorated this (26.85 ± 0.83 mm Hg, $P < 0.05$ vs. HPRX, Figures 4E and Figure E2C). Similarly, the RV:BW of the HYRX-control group was elevated compared with NRMX-control (0.85 ± 0.06 vs. 0.77 ± 0.02 for NRMX, $P < 0.05$) as was the Fulton's index (0.26 ± 0.015 vs. 0.22 ± 0.007 for NRMX, $P < 0.05$; Figures 4F and Figure E2D). MSC-exo treatment ameliorated the modest increase in RV:BW (0.77 ± 0.05, $P < 0.05$ vs. HYPRX-control). Fulton's index showed a decrease with MSC-exo treatment that was statistically significant for the BMSC-exos (Figure E2D).

Across all experimental groups, the degree of vascular remodeling (α-smooth muscle actin staining) was significantly associated with RV:BW ($P = 0.002$, $r = 0.807$), Fulton's index ($P = 0.001$, $r = 0.69$), and RVSP ($P = 0.002$, $r = 0.806$).

MSC-exo Treatment Improves Lung Function after HYRX-induced Lung Injury

To determine the functional impact of altered lung architecture and fibrosis, we performed pulmonary function testing in our experimental groups (NRMX-controls, HYRX-controls, and HYRX-exposed mice treated with WJMSC-exos) at PN42. In accordance with the lung histology (simplified alveolarization and emphysema-like features of lung disease), HYRX-exposed mice displayed an altered pressure–volume (PV) loop when compared with the NRMX-control group. PV loops in the HYRX-control group were shifted upwards and to the left, indicative of emphysema-like features of lung disease and air trapping (26). HYRX-control mice had an elevated total lung capacity (1.36 ± 0.04 ml), compared with the NRMX-control group (0.77 ± 0.04 ml, $P < 0.0001$), which was ameliorated by WJMSC-exo treatment (1.18 ± 0.02 ml, $P < 0.01$; Figure 4G). Exosome treatment improved the HYRX-induced emphysematous changes, significantly shifting the PV loop downward and to the right (Figure 4H). Airway resistance was not different between the groups; however, the HYRX-control mice had an elevated baseline compliance measurement that was not affected by MSC-exo treatment (not shown).

WJMSC-exos Modulate the Lung Transcriptome and Blunt HYRX-induced Inflammation

We opted for whole-organ RNA sequencing to generate an unbiased overview of the impact of WJMSC-exo treatment on the lung transcriptome, and to identify markers that could serve as potency metrics of exosome preparations through simple and expedient qPCR assays (Figures E3A–E3F). At PN7, HYRX-exposed animals had 2,561 significantly enriched and 2,344 suppressed mRNAs compared with their NRMX counterparts. WJMSC-exo treatment suppressed a subset of the HYRX-induced genes (117 mRNAs), and upregulated 83 genes that were suppressed by HYRX exposure, shifting the overall transcriptome profile toward the NRMX group (Figure 5A). Interestingly, 41 genes were specifically induced by WJMSC-exo treatment, and not by HYRX. Gene ontology analysis indicated these genes are likely involved in extracellular matrix and structural organization, cardiovascular

Figure 3. (Continued). by collagen deposition in the septal area. Compared with the emphysema-like appearance of HYRX-control animals, mice that received Wharton's jelly MSC (WJMSC)-exos or bone marrow MSC (BMSC)-exos presented with a restored alveolar development that was akin to the normoxic (NRMX) controls (H&E stain). Assessing collagen deposition, HYRX-controls had a modest, but significant, increase in septal collagen deposition when compared with NRMX-controls, as highlighted by arrows (Masson's trichrome stain). Levels were restored to NRMX-controls in HYRX-exposed mice that received either WJMSC-exos or BMSC-exos. Quantification of alveolar simplification was performed by measuring the mean linear intercept (MLI). Collagen deposition was used as a surrogate of fibrosis and was reported as percent of septal area. Each bar represents an experimental group, indicated on the *x*-axis and by the accompanying (+ or −) symbol. Data are shown as mean ± SEM; $n = 4$–5 per group. $^{*}P < 0.05$, $^{**}P < 0.01$, $^{***}P < 0.001$, $^{****}P < 0.0001$. H&E scale bars = 100 μm. Masson's trichrome scale bars = 50 μm.

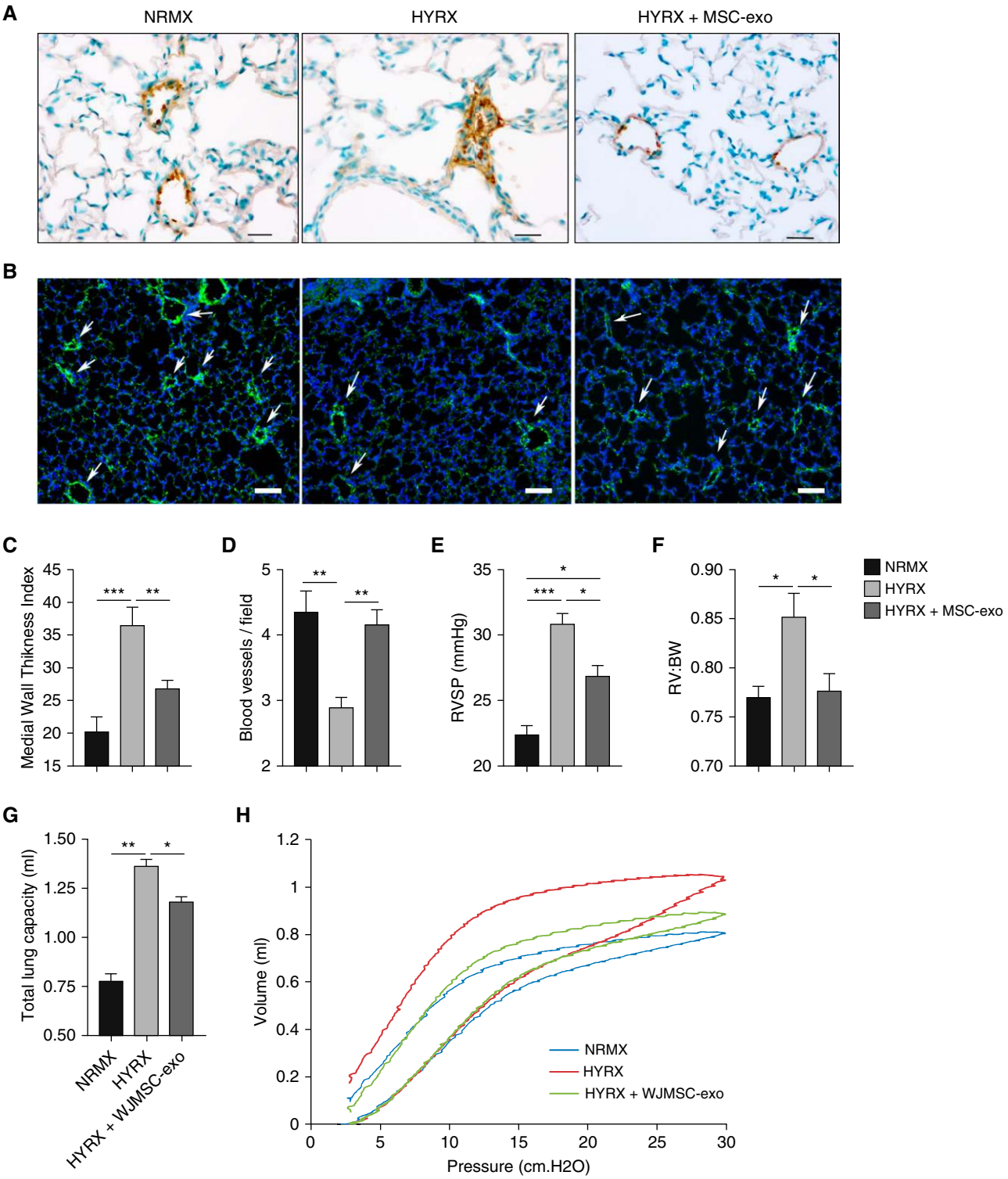

Figure 4. Mesenchymal stem/stromal cell (MSC) exosome (-exo) administration ameliorates pulmonary hypertension, prevents hyperoxia (HYRX)-induced loss of microvasculature, rescues peripheral pulmonary arterial remodeling, and improves lung function after HYRX-induced lung injury. With minimal evidence to suggest differences between Wharton's jelly MSC (WJMSC)-exo and bone marrow MSC (BMSC)-exo treatments, regarding their beneficial effects on long-term lung architecture, fibrosis, and pulmonary vasculature, our exosome treatments (WJMSC-exos and BMSC-exos) were plotted together and referred to as MSC-exo. (*A* and *C*) To assess the potential impact of MSC-exos on HYRX-induced peripheral pulmonary vascular remodeling, lung sections of mice harvested at Postnatal Day (PN) 42 were stained with α-smooth muscle actin. Increased pulmonary vascular remodeling was evident in HYRX-controls compared with their normoxic (NRMX) counterparts. MSC-exo treatment blunted the HYRX-induced increase in pulmonary vascular

development/morphogenesis, and SMAD protein import into the nucleus (Figure E3C).

Using gene ontology analysis, we found that HYRX exposure upregulated genes involved in the adaptive immune response, inflammatory response, and leukocyte-mediated immunity (Figure E3D). WJMSC-exo treatment blunted the hyperoxic induction of genes involved in inflammation, adaptive immune responses, IFN-γ–mediated signaling, and granulocyte and cytokine production (Figure E3E). In contrast to PN7, fewer changes in the lung mRNA profile were detected at PN14 (Figure E3B). HYRX-control mice had 356 upregulated and 282 suppressed mRNAs when compared with their NRMX counterparts. WJMSC-exo–treated mice presented modulated levels of a subset of HYRX-dysregulated genes (Figure E3F).

MSC-exos Suppress Inflammation by Immunomodulation of Macrophage Phenotype *In Vitro* and *In Vivo*

RNA-seq data were validated by qPCR using independent experimental groups treated with either WJMSC-exos or BMSC-exos. The results for a small panel of cytokines are plotted as one combined "MSC-exos" group in Figure 5B, and graphs depicting the effect of either WJMSC-exo or BMSC-exo preparations can be found in Figure E4. Cytokines, such as *Ccl2*, *Ccl7*, and *Il6*, typically associated with a proinflammatory macrophage programming, often denoted as "M1-like," as well as genes such as *Arg1* (arginase-1), *Cd206*, and *Ccl17*, typically associated with an antiinflammatory, proreparative/proremodeling programming, often denoted as "M2-like," were dysregulated in the hyperoxic lung, and were efficiently suppressed by the treatment.

We next assessed the ability of WJMSC-exos to regulate macrophage phenotype *in vitro*. Using fluorescence microscopy we observed WJMSC-exos were readily taken up by alveolar macrophages (Figure E5A). We then determined whether WJMSC-exos could regulate key macrophage genes as assessed by RT-qPCR. In a dose-dependent manner, the addition of WJMSC-exos to classically activated (M1) bone marrow–derived macrophages significantly reduced the mRNA levels of established proinflammatory M1 markers, such as *Tnfα*, *Il6*, and *Ccl5* ($P < 0.05$; Figure 6A). The addition of WJMSC-exos to M2 polarized macrophages significantly suppressed Retnla and *Cd206* induction ($P < 0.001$ and $P < 0.01$, respectively; Figure 6B), and greatly enhanced macrophage *Arg1* expression levels. Responses were dose dependent, and HDF-exos used as a vehicle and biologic control demonstrated minimal effect (Figure E5B).

In our HYRX-induced BPD model, flow cytometry was used to assess lung macrophage (*Cd45*$^{+ve}$, *Cd11b*$^{-ve}$, *Cd11c*$^{+ve}$, *Cd64*$^{+ve}$) phenotype *in vivo* at PN7 and PN14 (Figures 6C and 6D, Figure E6). *Cd40* and *Cd86* were used as markers for the proinflammatory "M1-like" phenotype, whereas *Cd206* was used as marker for the antiinflammatory, proremodeling "M2-like" phenotype. Akin to our *in vitro* results using bone marrow–derived macrophages and the observed lung transcriptome modulation *in vivo*, WJMSC-exos significantly suppressed the hyperoxic induction of *Cd206* levels at PN7 ($P < 0.05$), a trend that continued to PN14 ($P < 0.01$). At PN7 and PN14, *Cd40* levels were elevated in HYRX-control compared with their NRMX counterparts. This increase was suppressed by WJMSC-exo treatment at PN14, and, although a similar trend was observed at PN7, it was statistically nonsignificant. We found no difference in *Cd86* levels across all groups at both PN7 and PN14.

Discussion

Our results should be judged in the context of the experimental model we used. Several animal models have been developed, and continue to be refined, aiming to recapitulate pathological pulmonary hallmarks noted in lungs of human neonates with BPD. Although every preclinical model of BPD is subject to its own advantages and limitations, arguably BPD is most commonly modeled in mice. Reasons for this are manifold, and include relatively short gestation times allowing expedient studies on lung development. Importantly, the saccular stage of murine lung development occurs between Embryonic Day 17.5 and PN5. Therefore, term mouse lungs present a development stage resembling that of a human preterm neonate between 24 and 28 weeks gestation. This represents an excellent model for developmental lung injury, recently reviewed in Reference 27. We should note significant differences, however. Term mouse lungs, albeit in the saccular stage, are competent for proper gas exchange, whereas human preterm neonates often require supplemental oxygen and surfactant administration. Notwithstanding such divergence, the model used in this study presents significant alveolar simplification and subtle elevation in indices of secondary PH, closely resembling the human phenotype of "new" BPD.

Using this model, we demonstrate that a bolus dose of purified human exosomes, from either BMSCs or WJMSCs, effectively alleviates and rescues core features of HYRX-induced BPD, even after the injury

Figure 4. (Continued). remodeling. Images were taken at 400× magnification. Medial thickness index = 100× ($area_{[ext]} - area_{[int]}$) / $area_{[ext]}$). $Area_{[ext]}$ and $area_{[int]}$ denote the areas within the external and internal boundaries of the α-smooth muscle actin layer, respectively. Data are shown as mean ± SEM; $n = 4$–10 per group. Scale bars = 50 μm. (*B* and *D*) MSC-exos prevent HYRX-induced loss of blood vessels in the peripheral microvasculature. Lung sections were stained for von Willebrand factor (vWF) in mice harvested at PN42. vWF-positive vessels between 25 and 150 μm outer diameter were counted at 100× magnification in 8–12 random views, as described under Methods. Representative immunofluorescence staining shows a significant loss of small vessels (<50 μm diameter) in HYRX-exposed compared with NRMX-control mice, and a protective effect of MSC-exos in small (<50 μm) vessel number. Data are shown as mean ± SEM; $n = 5$–10 per group. Scale bars = 100 μm. Arrows highlight vWF-stained pulmonary vessels. To quantify the degree of pulmonary hypertension, we undertook direct right ventricular (RV) systolic pressure (RVSP) measurements (*E*) and assessed RV to body weight (BW) ratio (RV:BW) (*F*). Data are shown as mean ± SEM; $n = 6$–12 per group. In a separate experiment, pulmonary function testing was performed on mice harvested at PN42. Here, NRMX-control, HYRX-control, and HYRX + WJMSC-exo experimental groups were assessed. Total lung capacity (*G*) and pressure–volume (PV) relationships (*H*) were measured. Representative PV loops demonstrate a significant shift upward and to the left for the HYRX-control animals (red trace), indicative of emphysema-like features of lung disease and air trapping when compared with NRMX-controls (blue trace). HYRX-exposed animals that received a single dose of WJMSC-exos (green trace) showed a significant shift in PV loops downward and to the right (*H*). Data are shown as mean ± SEM; $n = 5$–8 per group. $^{*}P < 0.05$, $^{**}P < 0.01$, $^{***}P < 0.001$.

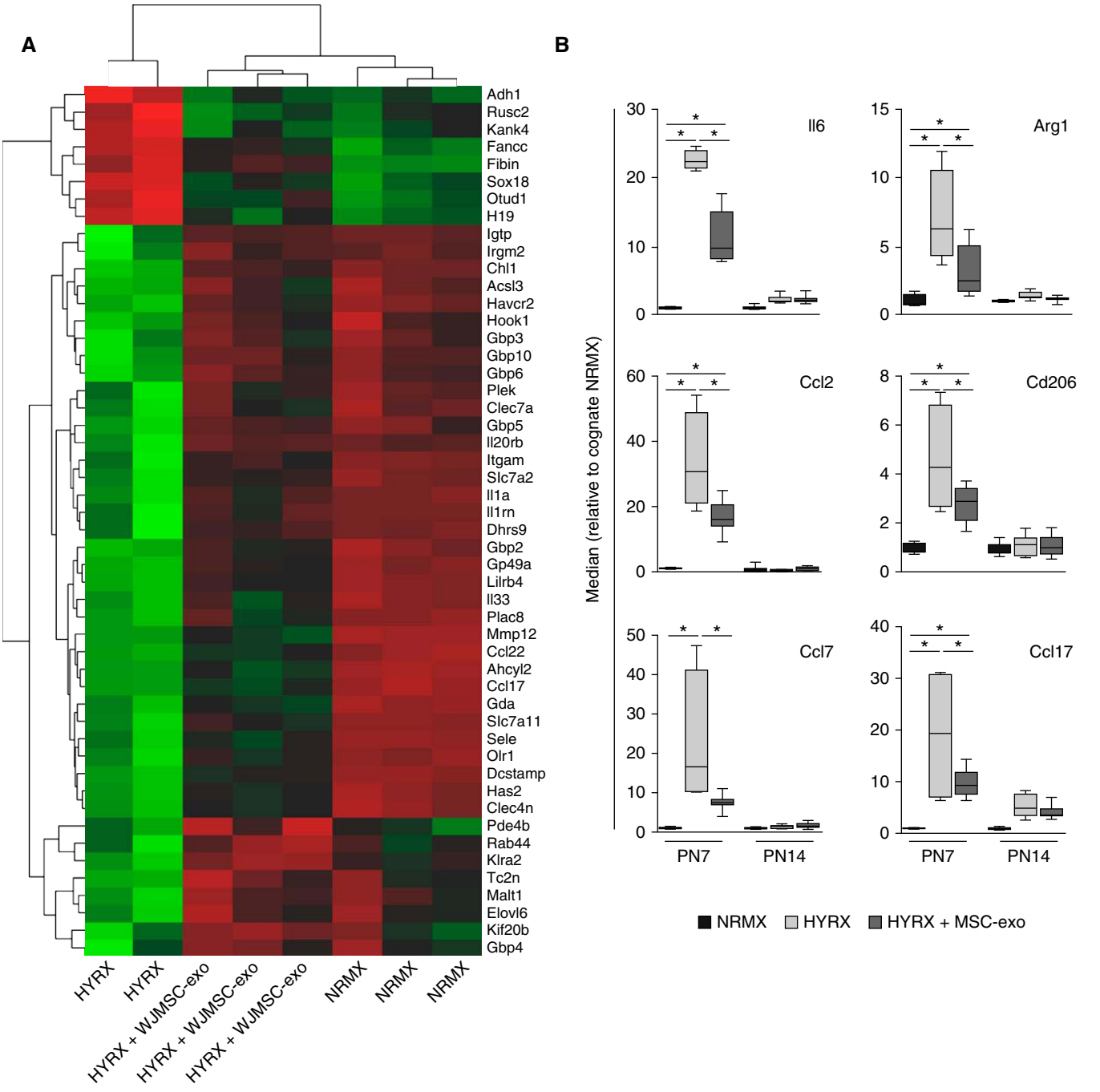

Figure 5. Wharton's jelly mesenchymal stem/stromal cell (WJMSC) exosome (-exo) treatment modulates hyperoxic lung transcriptome and blunts hyperoxia (HYRX)-induced inflammation. (*A*) Poly-A capture RNA-seq of mouse lung tissue at Postnatal Day (PN) 7 was performed on a subset of normoxic (NRMX)-control animals ($n = 3$), HYRX-control animals ($n = 2$), and WJMSC-exo–treated mice ($n = 3$). The heatmap shows the top 50 differentially expressed genes (red [−1] to green [+1] through black) ranked by adjusted *P* value at PN7. (*B*) Validation of select whole-lung RNA-seq data and suppression of candidate proinflammatory markers by MSC-exo treatment was assessed by RT-quantitative PCR in separate experiments. Here, our exosome treatments (WJMSC-exos and bone marrow MSC-exos) were plotted together and referred to as MSC-exo. Data are shown as median (minimum–maximum); $n = 4$–8 per group. $^*P < 0.05$.

has commenced. Specifically, we are the first to show that MSC-exo treatment radically improved lung morphology and pulmonary development, decreased lung fibrosis, rescued pulmonary vasculature loss, and ameliorated pulmonary vascular remodeling. We extend our observations to show that the cytoprotective actions of MSC exosomes result in desirable functional outcomes, such as improved pulmonary function test results and amelioration of associated PH. MSC-exos blunt proinflammatory signaling and immune responses in the hyperoxic lung via modulation of lung macrophage phenotype.

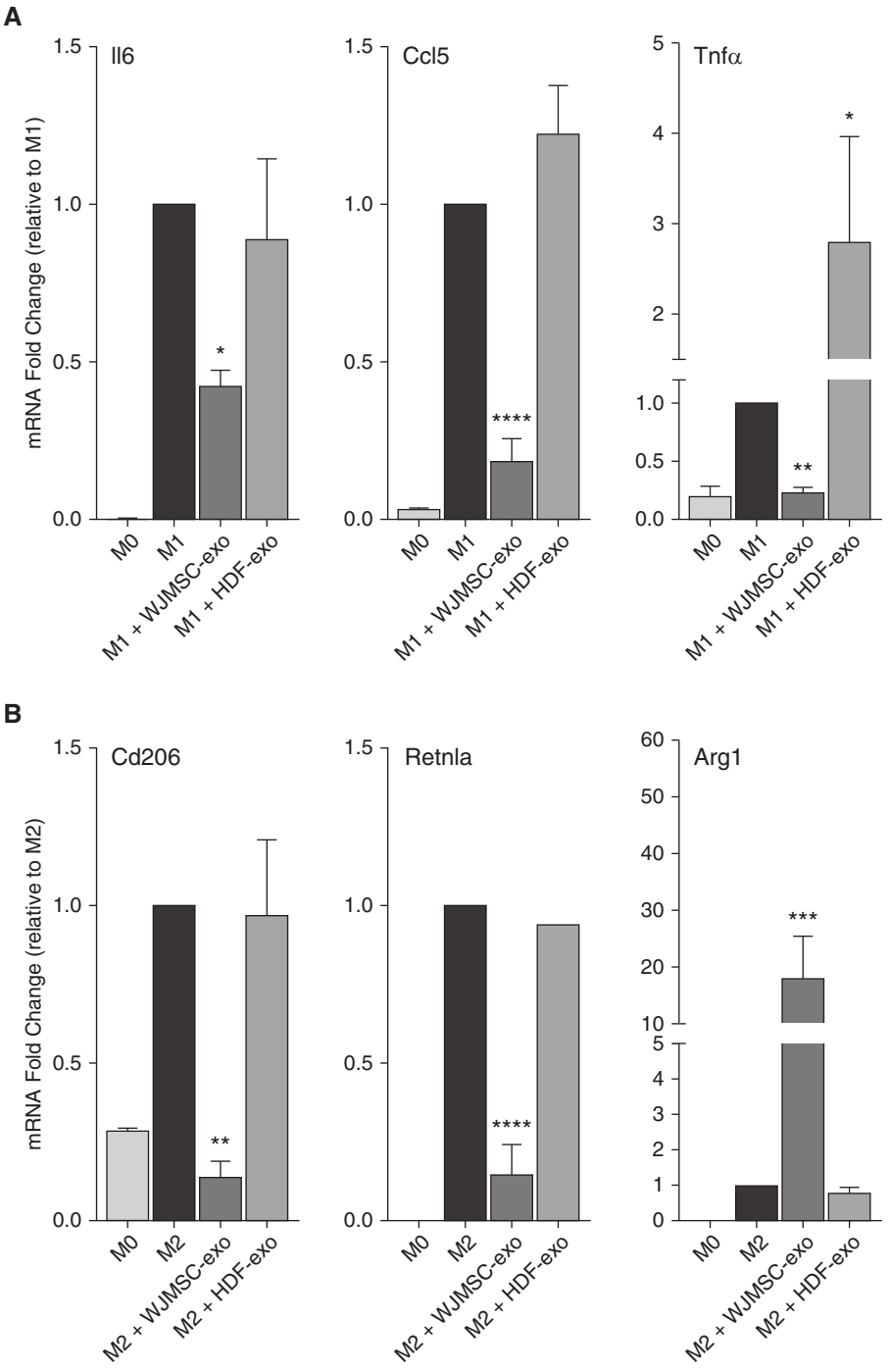

Figure 6. Immunomodulatory capacity of Wharton's jelly mesenchymal stem/stromal cell (WJMSC) exosomes (-exos): macrophage polarization potency assay. Macrophage polarization plays an important role in regulating the immune response and inflammation in the developing lung. The addition of WJMSC-exos to mouse bone marrow–derived macrophages or alveolar macrophages polarized to the proinflammatory M1 phenotype reduced the mRNA induction of markers, such as *Il6*, *Ccl5*, and *Tnfα* (*A*). The addition of WJMSC-exos to alternatively (M2) polarized macrophages super-induced arginase (*Arg*)-1 mRNA and modulated resistin-like alpha (Retnla) and *Cd206* induction (*B*). Flow cytometry was used to assess lung macrophage ($Cd45^{+ve}$, $Cd11b^{-ve}$, $Cd11c^{+ve}$, $Cd64^{+ve}$) phenotype. M1 markers, *Cd40* and *Cd86*, as well as M2 marker, *Cd206*, were assessed at Postnatal Day (PN) 7 and PN14. Median fluorescence intensity (MFI) was recorded (*C*). Representative histograms for *Cd40*, *Cd86*, and *Cd206* (*D*). Data are shown as mean ± SEM; $n = 4$–8 per group. HDF = human dermal fibroblasts; HYRX = hyperoxia; NRMX = normoxia. $^{*}P < 0.05$, $^{**}P < 0.01$, $^{***}P < 0.001$, $^{****}P < 0.0001$ versus M1 or M2 controls.

Our previous studies demonstrated that the MSC secretome is able to reverse core features of pathology in the neonatal mouse BPD model (6) even after severe injury subsequent to prolonged hyperoxic exposure (14). The current report identifies the therapeutic vector as exosomes, because a single dose of human MSC-exos suffices to ameliorate alveolar simplification, vascular remodeling and pulmonary blood vessel loss, and to blunt lung fibrosis and parameters of PH in our model. Complementing these findings, our study also shows that MSC-exo treatment results in significant long-term benefits in pulmonary function, improving PV loops and reducing total lung capacity. This is most relevant, as lung function abnormalities of infants with BPD often persist throughout childhood, and even into early adolescence. Consequently, this population exhibits increased risk in developing chronic obstructive pulmonary disease (28–30).

Inflammatory pathways are dysregulated in BPD (31, 32), and macrophages are critical mediators of the lung immune response, participating in both the initiation and the resolution of inflammation (33–36). Macrophage phenotypes are diverse, representing the impact of multidimensional networks on development, activation, and functional diversity (37, 38). The traditional M1/M2 binary paradigm is considered obsolete (39), and, indeed, recent elegant studies in preclinical models stress the effects of microenvironment on pulmonary macrophage plasticity and address the diversity of temporal and compartmental macrophage phenotypes in relation to lung homeostasis and disease (35, 36, 40).

MSC-exos have been recognized as potent immunomodulators (for reviews, *see* References 24, 41–43), and our study suggests that they can modulate the pulmonary macrophage phenotype fulcrum, as evidenced by the expression of markers associated with proinflammatory "M1-like" states and antiinflammatory, proremodeling, "M2-like" states. We suggest that the impact of MSC-exo on pulmonary macrophage phenotype underlies their therapeutic action through the modulation of the HYRX-induced inflammation in the neonatal lung. At PN14, when exposed animals had already been returned to room air for a week, most

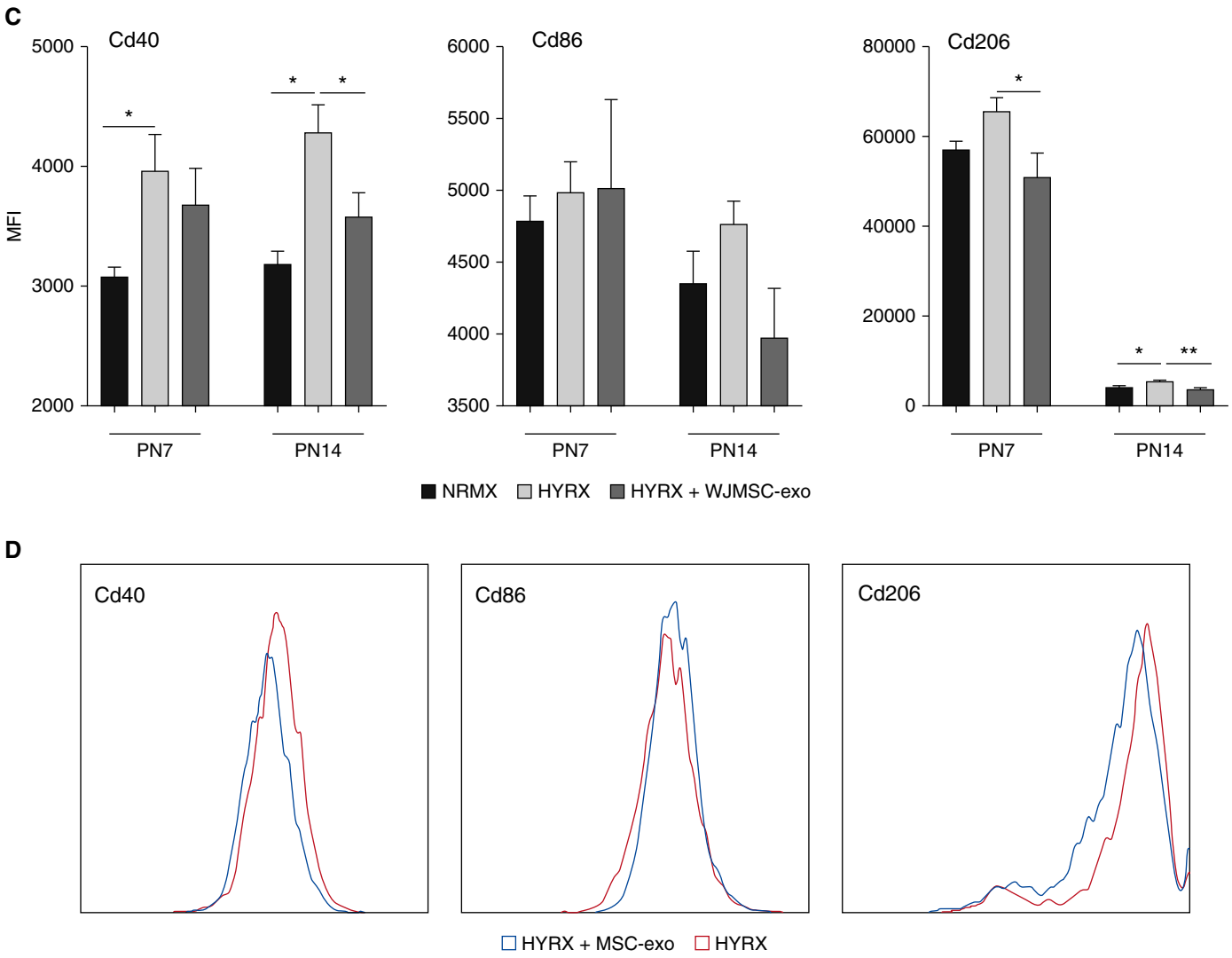

Figure 6. (Continued).

(albeit not all) of the HYRX-induced dysregulation of lung gene expression had returned to normal, suggesting that early intervention and blunting the early HYRX-induced inflammatory phase is critical for preserving proper lung development.

Elucidation of the molecular mechanisms of MSC-exo action is pending. Nevertheless, recent studies reported that MSCs release EVs containing mitochondria, and EV-mediated mitochondrial transfer may alter macrophage phenotypes (23, 44). However, the mitochondrial transfer vector appears to be microvesicles larger than 500 nm in diameter. Our density-purified exosome preparations, as assessed by TEM and size-exclusion chromatography (45) are comprised of particles less than 150 nm, and the majority is under 100 nm. Although the possibility cannot be formally excluded, we consider it unlikely that the smaller particles studied here could encompass intact mitochondria (typically >1 μm).

We acknowledge several limitations of this work. We used here only one dose of MSC-exos, guided from the results of our previous studies using either MSC CM or exosomes (6, 14, 17); our rationale is further discussed in the online supplement. Future studies should determine dose responses, investigate functional-potency assays to standardize exosome dosing, and investigate different routes/timings of administration. The biodistribution and metabolic fate of administered MSC-exos remain unclear and warrants further scrutiny. In this study, RNA sequencing was performed on whole-lung mRNA to define a broad base and to identify markers that could be used as metrics of the potency of MSC-exo preparations in simple and expedient assays. Future studies should profile sorted cell subtypes to assess the effect of MSC-exos on different target cell populations and address the molecular mechanisms underlying their therapeutic action.

With the recognition that MSC action can be predominately paracrine, MSC-exo–based therapies may be perceived as highly advantageous over live cell–based therapies. MSC-exos are considered less immunogenic than their parental cells (46), and exosome administration mitigates many of the safety concerns and limitations

associated with administration of viable cells. Exosome vectors can also be modified (47) to enhance bioavailability and cell targeting, and, because exosomes can be stored frozen with no loss of activity, they can be the basis of expedient and economical drug formulations, as "off-the-shelf" products. However, the above appraisal may be an oversimplification. MSC action may not be restricted to strict paracrine mechanisms (including the <150-nm exosome vectors), but may also involve transfer of higher-complexity components, including mitochondria, either by microvesicles (>500 nm in diameter) or by tunneling tubes requiring cell-to-cell contact (23, 44, 48, 49). Although in the animal models of disease with which we work, efficacy of purified exosome administration is equal or superior to that of live MSCs, the possibility that certain pathologies could respond better (or even exclusively) to live MSC therapies cannot be presently excluded, and any conjectures on the topic can only be speculative.

In conclusion, we purified and carefully characterized exosomes derived from human WJMSCs, BMSCs, and HDF-exos, and demonstrated a robust therapeutic effect in a BPD model that is specific to exosomes of MSC origin. Importantly, we demonstrate, for the first time, that purified MSC-exos are the major paracrine antiinflammatory and therapeutic mediators of MSC action in the hyperoxic lung. MSC-exos act, at least in part, through modulation of the lung macrophage phenotype, suppressing lung inflammation and immune responses to favor proper organ development. Given the recognized pleiotropic effects of MSC-exos (41), other prematurity-associated pathologies, including neurological injury, could, in the very near future, be the targets of exosome-based therapies. ■

Author disclosures are available with the text of this article at www.atsjournals.org.

Acknowledgment: The authors thank Carolina Medrano and Dr. Roger Ilagan at United Therapeutics Corp. for providing mesenchymal stem/stromal cell conditioned media and many useful discussions. They also thank Dr. Lui Bao for his expert technical assistance with the pulmonary function tests, John Daley II for his cytometry expertise and technical assistance, and Dr. Henry Feldman for his input on statistical analyses.

References

1. Jobe AH, Bancalari E. Bronchopulmonary dysplasia. *Am J Respir Crit Care Med* 2001;163:1723–1729.
2. Stenmark KR, Abman SH. Lung vascular development: implications for the pathogenesis of bronchopulmonary dysplasia. *Annu Rev Physiol* 2005;67:623–661.
3. Baraldi E, Filippone M. Chronic lung disease after premature birth. *N Engl J Med* 2007;357:1946–1955.
4. Khemani E, McElhinney DB, Rhein L, Andrade O, Lacro RV, Thomas KC, *et al*. Pulmonary artery hypertension in formerly premature infants with bronchopulmonary dysplasia: clinical features and outcomes in the surfactant era. *Pediatrics* 2007;120:1260–1269.
5. del Cerro MJ, Sabaté Rotés A, Cartón A, Deiros L, Bret M, Cordeiro M, *et al*. Pulmonary hypertension in bronchopulmonary dysplasia: clinical findings, cardiovascular anomalies and outcomes. *Pediatr Pulmonol* 2014;49:49–59.
6. Aslam M, Baveja R, Liang OD, Fernandez-Gonzalez A, Lee C, Mitsialis SA, *et al*. Bone marrow stromal cells attenuate lung injury in a murine model of neonatal chronic lung disease. *Am J Respir Crit Care Med* 2009;180:1122–1130.
7. van Haaften T, Byrne R, Bonnet S, Rochefort GY, Akabutu J, Bouchentouf M, *et al*. Airway delivery of mesenchymal stem cells prevents arrested alveolar growth in neonatal lung injury in rats. *Am J Respir Crit Care Med* 2009;180:1131–1142.
8. Baker CD, Seedorf GJ, Wisniewski BL, Black CP, Ryan SL, Balasubramaniam V, *et al*. Endothelial colony-forming cell conditioned media promote angiogenesis *in vitro* and prevent pulmonary hypertension in experimental bronchopulmonary dysplasia. *Am J Physiol Lung Cell Mol Physiol* 2013;305:L73–L81.
9. Hodges RJ, Jenkin G, Hooper SB, Allison B, Lim R, Dickinson H, *et al*. Human amnion epithelial cells reduce ventilation-induced preterm lung injury in fetal sheep. *Am J Obstet Gynecol* 2012;206:448.e8–448.e15.
10. Kourembanas S. Expanding the pool of stem cell therapy for lung growth and repair. *Circulation* 2014;129:2091–2093.
11. Kourembanas S. Stem cell-based therapy for newborn lung and brain injury: feasible, safe, and the next therapeutic breakthrough? *J Pediatr* 2014;164:954–956.
12. Lee JW, Fang X, Krasnodembskaya A, Howard JP, Matthay MA. Concise review: mesenchymal stem cells for acute lung injury: role of paracrine soluble factors. *Stem Cells* 2011;29:913–919.
13. Liang OD, Mitsialis SA, Chang MS, Vergadi E, Lee C, Aslam M, *et al*. Mesenchymal stromal cells expressing heme oxygenase-1 reverse pulmonary hypertension. *Stem Cells* 2011;29:99–107.
14. Hansmann G, Fernandez-Gonzalez A, Aslam M, Vitali SH, Martin T, Mitsialis SA, *et al*. Mesenchymal stem cell–mediated reversal of bronchopulmonary dysplasia and associated pulmonary hypertension. *Pulm Circ* 2012;2:170–181.
15. Curley GF, Hayes M, Ansari B, Shaw G, Ryan A, Barry F, *et al*. Mesenchymal stem cells enhance recovery and repair following ventilator-induced lung injury in the rat. *Thorax* 2012;67:496–501.
16. Pierro M, Ionescu L, Montemurro T, Vadivel A, Weissmann G, Oudit G, *et al*. Short-term, long-term and paracrine effect of human umbilical cord–derived stem cells in lung injury prevention and repair in experimental bronchopulmonary dysplasia. *Thorax* 2013;68:475–484.
17. Lee C, Mitsialis SA, Aslam M, Vitali SH, Vergadi E, Konstantinou G, *et al*. Exosomes mediate the cytoprotective action of mesenchymal stromal cells on hypoxia-induced pulmonary hypertension. *Circulation* 2012;126:2601–2611.
18. Sdrimas K, Kourembanas S. MSC microvesicles for the treatment of lung disease: a new paradigm for cell-free therapy. *Antioxid Redox Signal* 2014;21:1905–1915.
19. van der Pol E, Böing AN, Gool EL, Nieuwland R. Recent developments in the nomenclature, presence, isolation, detection and clinical impact of extracellular vesicles. *J Thromb Haemost* 2016;14:48–56.
20. Cruz FF, Borg ZD, Goodwin M, Sokocevic D, Wagner DE, Coffey A, *et al*. Systemic administration of human bone marrow–derived mesenchymal stromal cell extracellular vesicles ameliorates aspergillus hyphal extract–induced allergic airway inflammation in immunocompetent mice. *Stem Cells Transl Med* 2015;4:1302–1316.
21. Monsel A, Zhu YG, Gennai S, Hao Q, Hu S, Rouby J-J, *et al*. Therapeutic effects of human mesenchymal stem cell–derived microvesicles in severe pneumonia in mice. *Am J Respir Crit Care Med* 2015;192:324–336.
22. Laffey JG, Matthay MA. Fifty years of research in ARDS: cell-based therapy for acute respiratory distress syndrome: biology and potential therapeutic value. *Am J Respir Crit Care Med* 2017;196:266–273.
23. Phinney DG, Di Giuseppe M, Njah J, Sala E, Shiva S, St Croix CM, *et al*. Mesenchymal stem cells use extracellular vesicles to outsource mitophagy and shuttle microRNAs. *Nat Commun* 2015;6:8472.
24. Kourembanas S. Exosomes: vehicles of intercellular signaling, biomarkers, and vectors of cell therapy. *Annu Rev Physiol* 2015;77:13–27.

25. Gennai S, Monsel A, Hao Q, Park J, Matthay MA, Lee JW. Microvesicles derived from human mesenchymal stem cells restore alveolar fluid clearance in human lungs rejected for transplantation. *Am J Transplant* 2015;15:2404–2412.
26. Suki B, Sato S, Parameswaran H, Szabari MV, Takahashi A, Bartolák-Suki E. Emphysema and mechanical stress–induced lung remodeling. *Physiology (Bethesda)* 2013;28:404–413.
27. Nardiello C, Mižíková I, Morty RE. Looking ahead: where to next for animal models of bronchopulmonary dysplasia? *Cell Tissue Res* 2017;367:457–468.
28. Schmalisch G, Wilitzki S, Roehr CC, Proquitté H, Bührer C. Development of lung function in very low birth weight infants with or without bronchopulmonary dysplasia: longitudinal assessment during the first 15 months of corrected age. *BMC Pediatr* 2012;12:37.
29. Stocks J, Hislop A, Sonnappa S. Early lung development: lifelong effect on respiratory health and disease. *Lancet Respir Med* 2013;1: 728–742.
30. Postma DS, Bush A, van den Berge M. Risk factors and early origins of chronic obstructive pulmonary disease. *Lancet* 2015;385:899–909.
31. Speer CP. Pulmonary inflammation and bronchopulmonary dysplasia. *J Perinatol* 2006;(26 suppl 1:S57–S62. [Discussion, pp. S63–S64.]
32. Ambalavanan N, Carlo WA, D'Angio CT, McDonald SA, Das A, Schendel D, *et al*.; Eunice Kennedy Shriver National Institute of Child Health and Human Development Neonatal Research Network. Cytokines associated with bronchopulmonary dysplasia or death in extremely low birth weight infants. *Pediatrics* 2009;123:1132–1141.
33. Viscardi RM. Perinatal inflammation and lung injury. *Semin Fetal Neonatal Med* 2012;17:30–35.
34. Laskin DL, Sunil VR, Gardner CR, Laskin JD. Macrophages and tissue injury: agents of defense or destruction? *Annu Rev Pharmacol Toxicol* 2011;51:267–288.
35. Johnston LK, Rims CR, Gill SE, McGuire JK, Manicone AM. Pulmonary macrophage subpopulations in the induction and resolution of acute lung injury. *Am J Respir Cell Mol Biol* 2012;47:417–426.
36. Pugliese SC, Kumar S, Janssen WJ, Graham BB, Frid MG, Riddle SR, *et al*. A time- and compartment-specific activation of lung macrophages in hypoxic pulmonary hypertension. *J Immunol* 2017;198:4802–4812.
37. Lawrence T, Natoli G. Transcriptional regulation of macrophage polarization: enabling diversity with identity. *Nat Rev Immunol* 2011; 11:750–761.
38. Ginhoux F, Schultze JL, Murray PJ, Ochando J, Biswas SK. New insights into the multidimensional concept of macrophage ontogeny, activation and function. *Nat Immunol* 2016;17:34–40.
39. Nahrendorf M, Swirski FK. Abandoning M1/M2 for a network model of macrophage function. *Circ Res* 2016;119:414–417.
40. El Kasmi KC, Stenmark KR. Contribution of metabolic reprogramming to macrophage plasticity and function. *Semin Immunol* 2015;27: 267–275.
41. Mitsialis SA, Kourembanas S. Stem cell–based therapies for the newborn lung and brain: possibilities and challenges. *Semin Perinatol* 2016;40:138–151.
42. Burrello J, Monticone S, Gai C, Gomez Y, Kholia S, Camussi G. Stem cell–derived extracellular vesicles and immune-modulation. *Front Cell Dev Biol* 2016;4:83.
43. Zhang B, Yin Y, Lai RC, Tan SS, Choo ABH, Lim SK. Mesenchymal stem cells secrete immunologically active exosomes. *Stem Cells Dev* 2014;23:1233–1244.
44. Morrison TJ, Jackson MV, Cunningham EK, Kissenpfennig A, McAuley DF, O'Kane CM, *et al*. Mesenchymal stromal cells modulate macrophages in clinically relevant lung injury models by extracellular vesicle mitochondrial transfer. *Am J Respir Crit Care Med* 2017;196: 1275–1286.
45. Willis GR, Kourembanas S, Mitsialis SA. Toward exosome-based therapeutics: isolation, heterogeneity, and fit-for-purpose potency. *Front Cardiovasc Med* 2017;4:63.
46. Yeo RW, Lai RC, Zhang B, Tan SS, Yin Y, Teh BJ, *et al*. Mesenchymal stem cell: an efficient mass producer of exosomes for drug delivery. *Adv Drug Deliv Rev* 2013;65:336–341.
47. Lai RC, Yeo RW, Tan KH, Lim SK. Exosomes for drug delivery—a novel application for the mesenchymal stem cell. *Biotechnol Adv* 2013;31: 543–551.
48. Islam MN, Das SR, Emin MT, Wei M, Sun L, Westphalen K, *et al*. Mitochondrial transfer from bone-marrow–derived stromal cells to pulmonary alveoli protects against acute lung injury. *Nat Med* 2012; 18:759–765.
49. Jackson MV, Morrison TJ, Doherty DF, McAuley DF, Matthay MA, Kissenpfennig A, *et al*. Mitochondrial transfer via tunneling nanotubes is an important mechanism by which mesenchymal stem cells enhance macrophage phagocytosis in the *in vitro* and *in vivo* models of ARDS. *Stem Cells* 2016;34:2210–2223.